Earth Planets Space, **55**, 315–326, 2003

On the role of oceans in the geomagnetic induction by Sq along the 210° magnetic meridian region

E. Chandrasekhar[1], Naoto Oshiman[1], and Kiyohumi Yumoto[2]

[1]*Research Center for Earthquake Prediction, Disaster Prevention Research Institute, Kyoto University, Gokasho, Uji, Kyoto 611-0011, Japan*
[2]*Department of Earth and Planetary Science, Kyushu University, Fukuoka 812-8581, Japan*

(Received November 29, 2002; Revised June 12, 2003; Accepted July 14, 2003)

We have utilized solar quiet daily variation (Sq) data recorded at a network of temporary and permanent magnetic observatories, operated along the western Pacific coast, in the 210° Magnetic Meridian (MM) region, spanning both hemispheres. The selected data sets correspond to solar-quiet year 1996. We have determined the ionospheric source current systems for all three Lloyd's seasons prior to calculating the Sq-induction response. As the selected data sets encompass the whole range of the western Pacific, we studied the role of self-induction effect (SIE) of the ocean at 24-hr period of Sq on the induction response, following the theory developed by Rikitake (1960). Our calculations show a considerable influence of the SIE on the induction response at 24-hr period, implying that ignoring the SIE in induction studies in oceanic regions leads to erroneous interpretation of the results. We have observed a large regional bias in the derived induction response estimates along the 210°MM region. As the ocean effect also depends on the regional subsurface structure and its conductivity, we believe that in addition to the SIE, the bias in the estimated response functions could be due to the strong influence of the coupling of the electric currents induced in the ocean and the highly heterogeneous upper mantle that has resulted from the active lithospheric convergence between the Pacific and Philippine Sea plates all along the western Pacific. We interpret the derived induction responses in the light of the tectonic significance of the 210°MM region. We also discuss the well-defined seasonal differences in ionospheric source current systems by comparing them with those reported for the East Asian sector.

Key words: Sq-induction, self-induction effect of the ocean, 210°MM region, western Pacific region.

1. Introduction

Understanding the role of oceans in global electromagnetic (EM) induction has been a longstanding problem. Chapman and Whitehead (1923) first laid down the theory for EM induction in a uniform conducting shell surrounding a uniform spherical core and showed a strong effect of the ocean on the internal part of geomagnetic variations. Later Price (1949) extended their theory to study induction of electrical currents in non-uniform thin sheets and shells. Following Price's work, Rikitake (1960) solved a boundary value problem approximating the Pacific ocean by a hemispherical sheet and showed that in the solution of oceanic induction problems at periods of one-day and below, the self-induction effect of the oceans must be taken into account (Kendall and Quinney, 1983). Bullard and Parker (1970) defined the ratio of the induced field to the inducing field as a measure of the self-induction in limiting the induced current. They showed that this ratio is small for seas and large for oceans and thus a study of the self-induction effect of the oceans is mandatory in solving oceanic induction problems, particularly at periods of a few days and below. Fainberg (1980) provided an excellent review of oceanic induction problems until 1980. Later, a few more studies concerning the ocean influence on induction due to a variety of geomagnetic variations have been made both in terms of theory (Beamish *et al.*, 1983; Fainberg *et al.*, 1990a) and numerical computations (Fainberg *et al.*, 1990b; Takeda, 1991). Recently, considering a realistic model distribution of oceans and continents, Weiss and Everett (1998), through finite element modelling of the long-period induction response, reported that the influence of oceans at periods greater than 2 days is not significant in the observed geographic variability of the induction responses. This implies that oceans show considerable influence on the induction response at periods of less than 2 days; these periods are of prime concern in the present study. They also have done an analysis to estimate the sensitivity of the surface induction response to upper mantle heterogeneities. Considering inhomogeneous shell models for land and ocean, Kuvshinov *et al.* (1999) presented global induction responses due to Sq and geomagnetic storm (Dst) time variations in the presence of oceans.

The oceanic influence in the form of an "ocean dynamo" effect on magnetic variations has been studied by Larsen (1968), Malin (1969, 1970) and a few references therein. Later, Winch (1981, 1989) explained the importance of the ocean dynamo effect in geomagnetic induction studies, in terms of the significant Sq phase angle differences between the induced and inducing fields. More recently, using space-based magnetic observation data, Maus *et al.* (2002), for the first time, have reported a significant ocean tidal dynamo effect and its implications in mapping crustal magnetization.

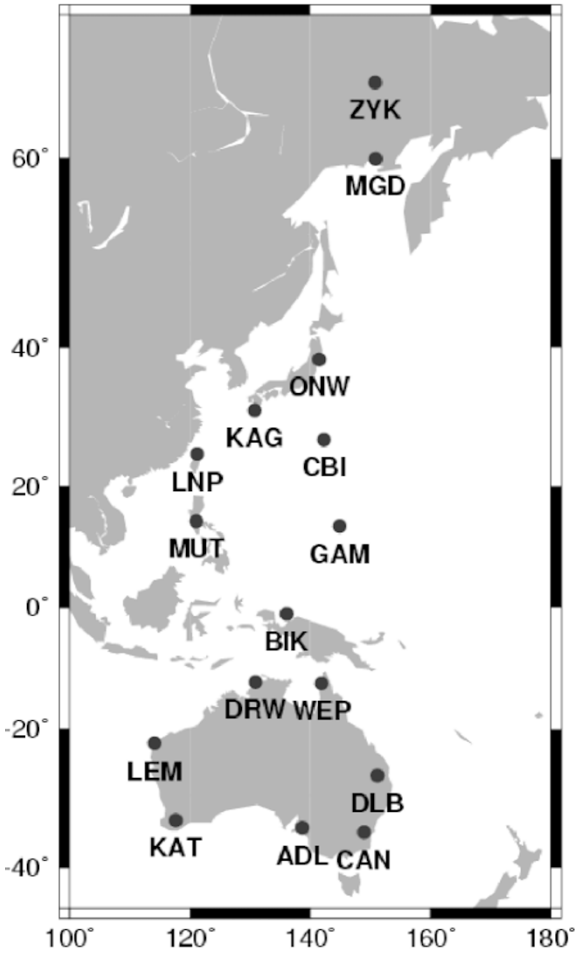

Fig. 1. Location of the magnetic observatories along the 110°–160° longitude band corresponding to the 210° magnetic meridian (MM) region whose data are utilized in the present study. (Note that the map is drawn in geographic coordinates). The Figure was drawn using the GMT software of Wessel and Smith (1995).

In general, the oceans affect Sq in two different ways. They act passively as an inductor, or actively as a dynamo due to ocean circulation. By the latter, the ocean acts as a dynamo in the same way as the ionosphere. The active ocean dynamo has dual sources, arising from lunar as well as solar magnetic variations. Its effect is significant at semi-diurnal period for lunar magnetic variations (Malin, 1970; Winch, 1989). In his classic paper, Malin (1970) gave a methodology for separating the lunar magnetic variations into parts of oceanic and ionospheric origins. This separation was rather difficult because the semi-diurnal component that arises from both the ocean dynamo as well as from the ionospheric source is equally dominant. The oceanic tidal motions cutting across the permanent magnetic field of the Earth induce electric currents in the oceans and beneath the ocean floor. It is very important to note here that the induction generated by the ocean dynamo is *different* from the ocean effect that is familiar in induction studies, in that the latter arises only due to the physical presence of the ocean as a region of relatively high conductivity.

Concerning the oceans acting passively as inductors, there is a school of thought, which regards the self-inductive effects of the ocean as transients (this can be seen from the Laplace transformation of a first order differential equation with oscillatory or step-function boundary conditions (Winch, 2002, personal communication)) and that, however big or small, they die down once a steady state is reached. However, the question is, can we really treat these self-induction effects as 'transients' and neglect them in oceanic induction studies?

In an attempt to answer this question, in this paper we have calculated Rikitake's (1960) hemispherical thin sheet model using statistically improved Gauss coefficients, which are obtained using data recorded at a number of magnetic observatories located along the 210°MM region and explain quantitatively the oceanic influence on the EM induction response at the diurnal period of Sq and its harmonics. We first discuss at length the details of the well defined ionospheric source current systems responsible for the generation of Sq. Next, we present a quantitative description of the self-induction effect of the ocean and its role in EM induction at the diurnal period of Sq. Finally, we discuss the interpretation of the regional Sq induction response determined for the 210°MM region.

2. The Magnetic Database

We have utilized three-component geomagnetic H, D and Z data sets corresponding to the solar quiet year 1996, recorded at a chain of magnetic observatories located along the 210°MM region. The original data sets were recorded at 1 min. interval, from which we have computed hourly mean values. The data from the selected observatory network encompasses the Australian, the western Pacific and the Japanese regions, covering both hemispheres in the geomagnetic latitude range 45°N–45°S. Figure 1 shows the observatory locations in the 110°–160° geographic longitude band, corresponding to the 210°MM region. A complete list of observatory names and their geographic and geomagnetic coordinates are given in Yumoto *et al.* (1996).

2.1 Selection of quiet days

Using the geomagnetic daily index Ap (procured from the World Data Centre (WDC-C2) for Geomagnetism, Kyoto University, Japan), we have selected quiet days with $Ap \leq 6$ (see Rangarajan, 1989). Also, by overlapping the ap (the linear three-hourly range index of true planetary logarithmic geomagnetic index, Kp) values of 3 consecutive days in a fashion that an arithmetic average of 4 ap values of the day before quiet day, 8 ap values of the quiet day and 4 ap values of the day following quiet day, not exceeding 6, we have selected some more days, defined as Q*-days (Schmucker, 1999). Determination of Q*-days is rather an "ad-hoc" approach to increase the number of plausible quiet days in statistical analysis of data. This procedure has yielded a total of 159 quiet days and 122 Q*-days.

3. Data Processing and Fourier Analysis

We have analyzed the combined quiet and Q*-days by first grouping them into the three Lloyd's seasons: Winter season (January, February, November and December); Equinoctial season (March, April, September and October); and Summer season (May, June, July and August). In the literature, they are also respectively denoted as d-, e- and j- seasons (see for example Chandrasekhar and Alex, 1996). Occasional in-

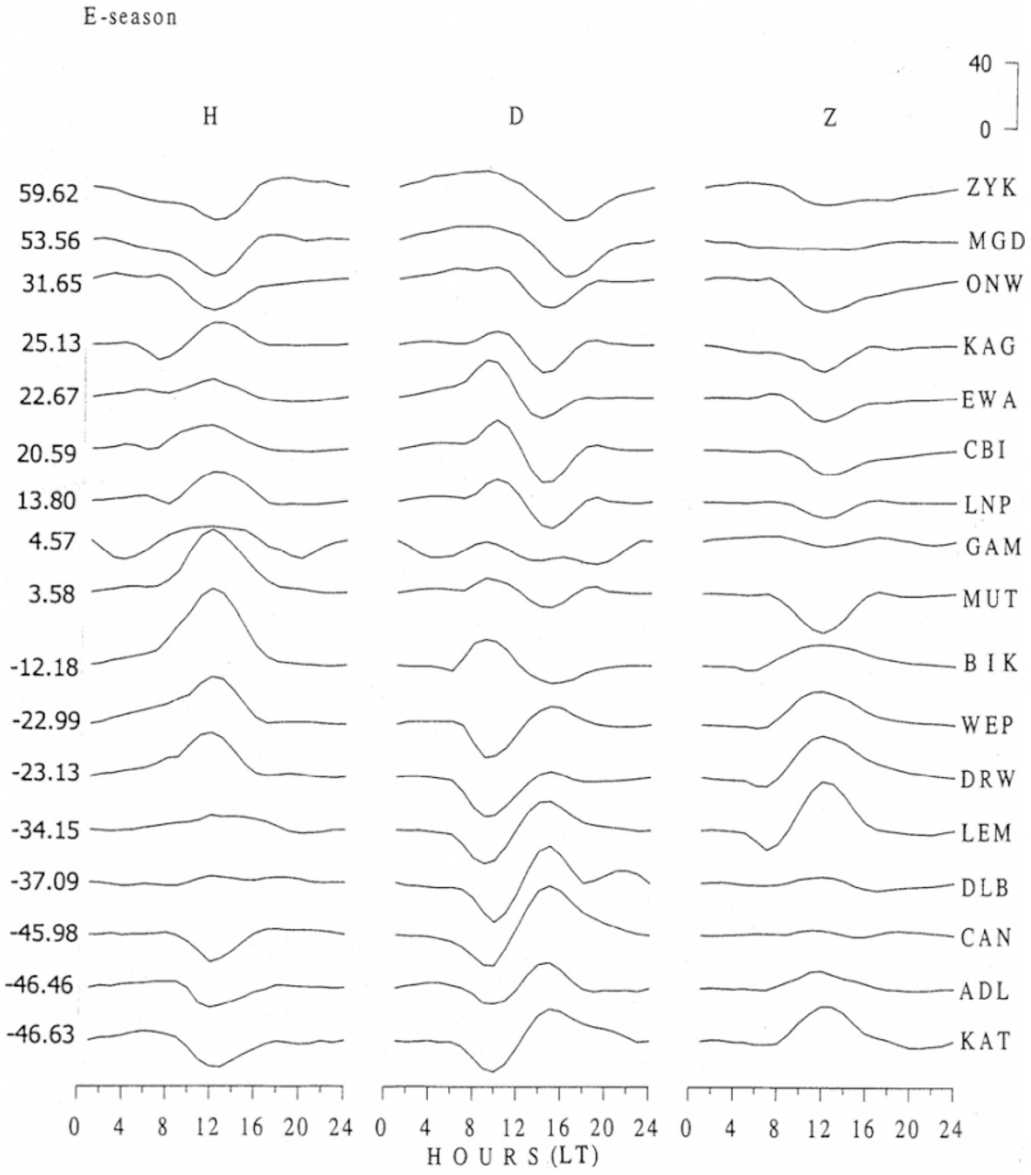

Fig. 2. Processed data of the averaged quiet-day geomagnetic H, D and Z variations (in nT) of all the stations, for E- (equinoctial) season. The geomagnetic latitude of the respective station is given on the left. The station EWA is not shown in Fig.1, as it is located eastwardly slightly away from the 210° longitude band, at the above latitude.

strument noise, baseline drifts, etc., that usually result in the form of box-like jumps in the data have been corrected prior to further analysis along with missing values and gaps. However, wherever spike-like jumps were present in the whole length of the data sequence of any component, we corrected those portions by visual inspection.

Next, we high-pass filtered the data sets to suppress the long-period background continuum noise and selected only those data sets with periods 1 day and below. We then applied a noncyclic correction to the data. Figure 2 shows an example plot of the fully processed data of all the stations for E (equinoctial)-season. We next have Fourier analyzed all the data sets. For the type of study described here, it is essential to ensure *a priori* the presence of periodicities in the data sets. Fourier analysis does this job of effectively identifying the hidden periodicities in the data. However, a question arises: Can we apply Fourier analysis to geomagnetic data, which in general are non-stationary? The answer is "yes", because in general, whether a given time series is stationary or non-stationary, if it satisfies at least one of the three Dirichlet's conditions (Spiegel, 1974), then that time series can be Fourier analyzed. However, the spectral resolution of periodicities will be good for stationary time series and poor for non-stationary time series. Figure 3 shows the power spectral plot of D, H and Z variations of one of the mid-latitude stations, LNP (Lunping). The computed Fourier spectra of all the data sets have clearly resolved the required periodicities in the data, in the form of distinct peaks at 24-, 12-, 8- and 6-hour periods, respectively corresponding to Sq and its first three harmonics. Using the spherical harmonic analysis technique detailed by Campbell and Schiffmacher (1985), we have separated the Sq field into external and internal parts. Spherical harmonic Gauss coefficients have been calculated up to maximum degree 12 and order 4. Figure 4 shows an example plot of the external and internal parts of H, D and Z variations for two mid-latitude stations correspond-

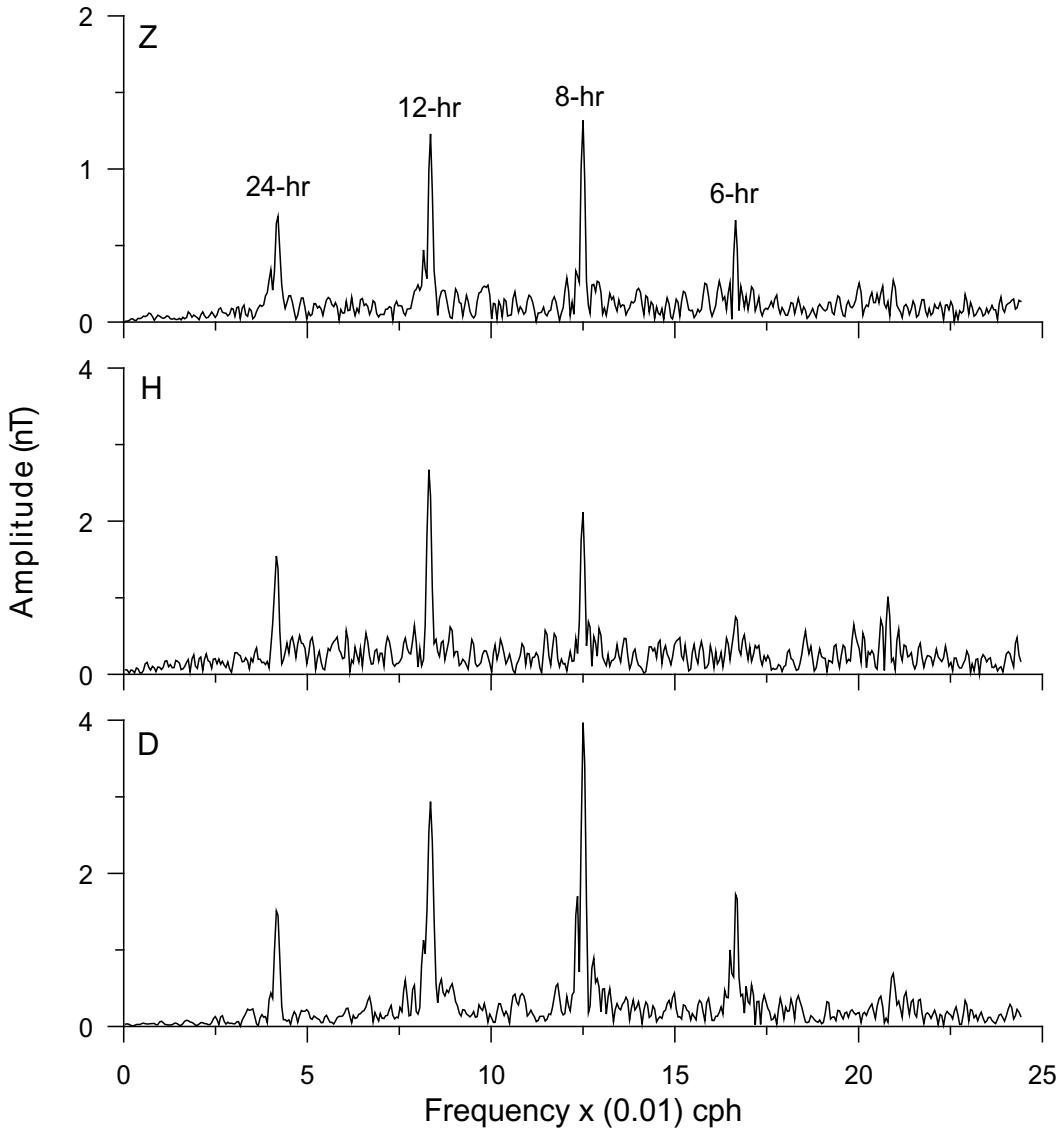

Fig. 3. Power spectral plots of D, H and Z variations for one of the mid-latitude stations, Lunping (LNP) for E- (equinoctial) season. Note the clear resolution of peaks at 24-, 12-, 8- and 6-hour periods, respectively corresponding to Sq and its first three harmonics.

ing to the northern (LNP) and the southern (WEP) (Wepia) hemispheres for E-season (see Fig. 1).

4. Determination of Equivalent Ionospheric Source Current Systems

As well known, the estimation of equivalent ionospheric source current systems helps to understand ionospheric thermo tidal motions, responsible for the generation of the Sq field. A clear characterization of the external source current system thus ensures: (i) the proper spherical harmonic separation of the observed field into external and internal parts; and (ii) the reliability of the EM induction response of the Earth, which in turn depends on the well-defined spatial structure of the inducing field. Therefore, to ensure a clear definition of the external source current systems, we have used the estimated Gauss external coefficients to determine the season-wise ionospheric source current systems for Sq (Fig. 5). The estimated spherical harmonic Gauss external coefficients of the first four principal harmonic terms of Sq are given in Appendix A.

5. Determination of the EM Induction Response of the Substitute Conductor Model and the Self-induction Effect of Ocean

Schmucker (1970) first developed a method to calculate the conductivity and depth estimates of a substitute conductor model by determining a complex transfer function, $C(\omega)$, using the spectral components of geomagnetic (vertical) Z and (horizontal) H field variations. Here, the real (or in-phase) part of $C(\omega)$ describes the depth of penetration of the inducing field and the imaginary (or quadrature) part of $C(\omega)$ is used to estimate the conductivity of the substitute conductor. A simple 2-layer model, in which, a resistive layer overlies an inner high conducting layer is defined as the substitute conductor model. Thus, if the EM responses over such a simple 2-layer model at a sequence of periods in any region are computed, then all the responses of the substitute conductor models corresponding to all the periods can be combined and modelled together, to calculate corresponding conductivity and depth estimates. This describes the overall regional conductivity-depth distribution of that

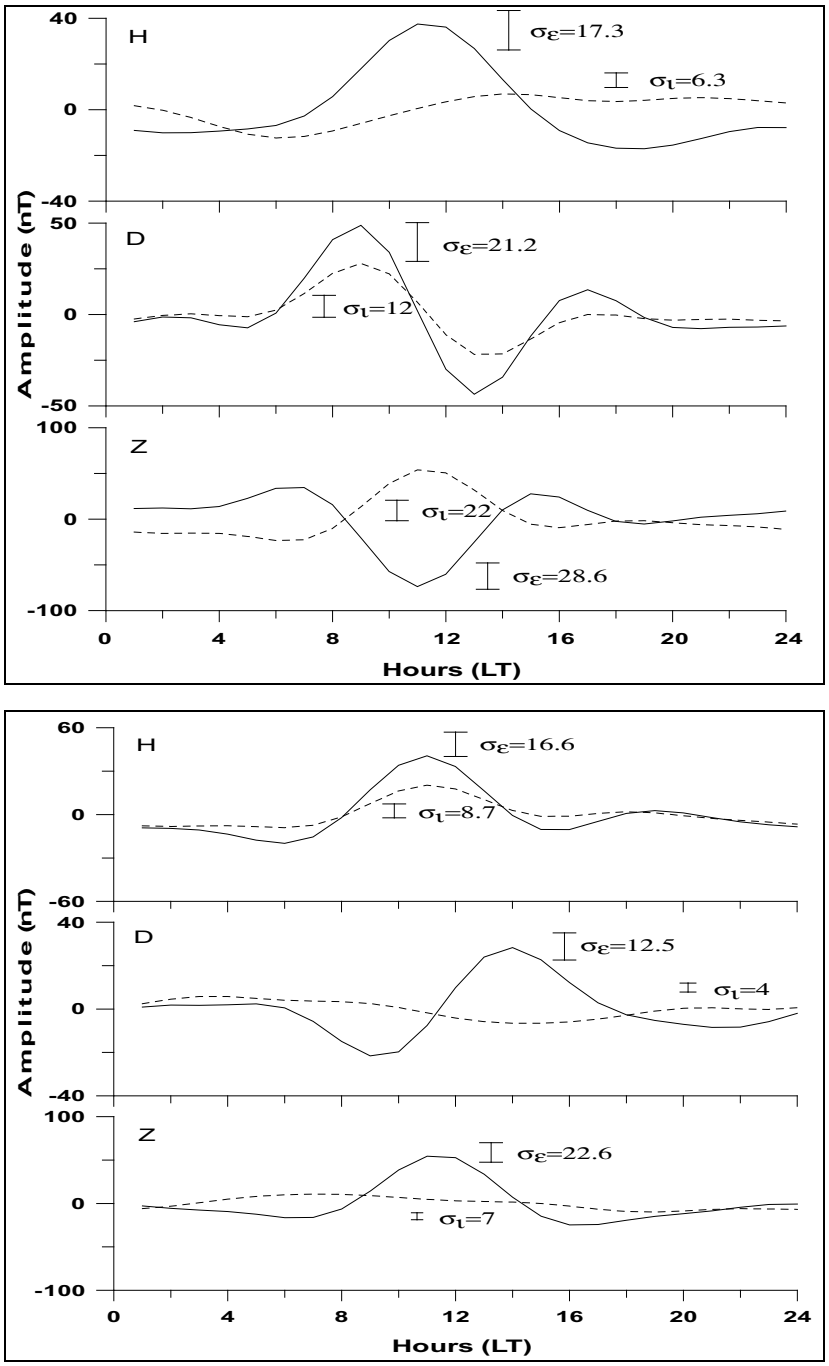

Fig. 4. Separated external (solid lines) and internal (dashed lines) parts of the H, D and Z variations for E-season, at 14°(N) geomagnetic latitude corresponding to LNP (top panel) and at 23°(S) geomagnetic latitude corresponding to WEP (bottom panel). In both the panels, the errors are shown as vertical bars that denote the sample standard deviations, σ_ϵ, for external and σ_ι, for internal field variations in nT.

region. Schmucker (1987) gave full details of the substitute conductor models for different EM response functions in his excellent review. Using the spectral components of geomagnetic Z and H fields, the long period EM induction responses have been calculated to provide the upper mantle electrical conductivity distribution for the European region (Olsen, 1998) and for the Indian and other global regions (Chandrasekhar, 2000 and references therein).

Campbell and Anderssen (1983) generalized the Schmucker's (1970) formulation and developed a method to estimate the complex C(ω)-response directly using the spherical harmonic Gauss coefficients for Sq induction studies. In the present study, we have employed Campbell and Anderssen's (1983) method and calculated induction response estimates, for the periods of Sq and its harmonics. The averaged conductivity, depth (together with their errors) and phase estimates for a substitute conductor model are given in Table 1.

As regards induction, it is of great concern, when the observatories are located directly at or near the ocean, as in the present case. When induction at periods of Sq, in large oceans such as Pacific, a study of the influence of the passive self-induction effect of the ocean is very important (Rikitake, 1960; Bullard and Parker, 1970; Kendall and Quinney,

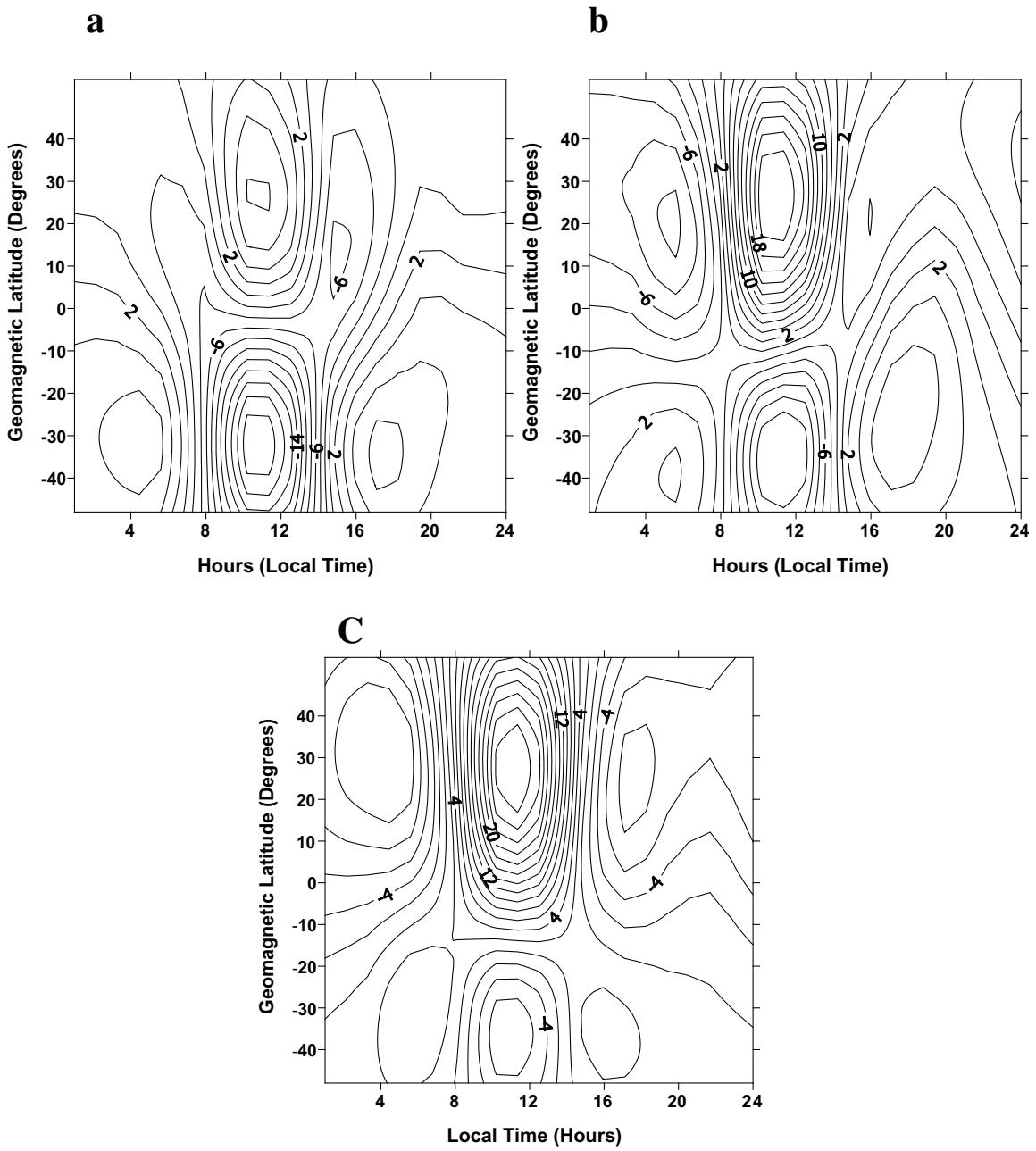

Fig. 5. Equivalent ionospheric source current system of Sq field in the 210°MM region for (a) winter, (b) equinoctial and (c) summer seasons. The current between the adjacent contours is 20 kA.

1983). Therefore, to examine the role of the self-induction effect of the ocean at 24-hr period of Sq on the estimated response, we have calculated the Rikitake (1960) model, which approximates the Pacific Ocean by a hemispherical thin sheet of uniform depth bounded by two meridians. Complete details of the theory and mathematical formulation are given in Rikitake's paper (See Appendix-B, which provides a few more steps that serve as a small addendum to Rikitake's (1960) formulation). For an assumed ocean depth of 1000 m and conductivity of 4 S/m, we have estimated the self-induction effect of the ocean for two cases: (i) when its contribution is not ignored; and (ii) ignored, in the calculations. Table 2 shows the obtained coefficients for induction due to the diurnal term of Sq, when the self-induction effect of the ocean is not ignored and Table 3 shows the list of these coefficients when the self-induction effects of the ocean are ignored.

6. Discussion

6.1 Equivalent ionospheric source current systems

Figure 4 shows the separated external and internal parts of the observed field for two midlatitude stations, LNP and WEP. The vertical bars in this figure represent the errors associated with the external and internal parts of the respective elements. The well-resolved external field has ensured a clear characterization of the source current systems responsible for the generation of Sq, as shown in Fig. 5. As evident from Fig. 5, there is no seasonal latitudinal shift of the Sq focus in both the hemispheres among different seasons. The Sq focus is located at around 25°-latitude in the

Table 1. Rough estimates of the complex C-response, depth, conductivity and phase, and their respective error estimates of the substitute conductor model for the periods of Sq and its harmonics along the 210°MM region. P_n^m harmonic terms of degree n and order m of the respective periods are given in parentheses in the first column.

Period in Hours	C-Response $(C_n^m = z - ip)$	Depth (km) $d_n^m = z - p$	Conductivity (S/m) $\sigma = \left(\frac{5.4 \times 10^4}{m(\pi \cdot p)^2}\right)$	Phase (Degrees) $\tan^{-1}(C_{imag}/C_{real})$
24 (P_2^1)	$325 - 281i$	606 (±355)	0.23 (±0.01)	−40.8
12 (P_3^2)	$496 - 63i$	559 (±220)	1.71 (±0.11)	−7.2
8 (P_4^3)	$349 - 47i$	396 (—)	0.82 (—)	−7.7
6 (P_5^4)	$129 - 114i$	243 (±45)	0.16 (±0.01)	−41.5

Table 2. Coefficients for the induction by the diurnal term of Sq for E-season, when the self-induction effect of the ocean is *not ignored.* a_n^- (a_n^*) and b_n^- (b_n^*) respectively denote real (imaginary) parts of the *cosine* and *sine* coefficients of the current functions of the induced electric currents at 24-hr period of Sq. For more details about the theory, mathematical part of these coefficients and their estimation, the reader is referred to Rikitake (1960) (see also Appendix B). These coefficients are obtained after solving the simultaneous equations (see equations 18 and 19 of Rikitake (1960)) using the Gauss external *cosine* and *sine* P_2^1 coefficients given in Table A.1 of Appendix A. The values correspond to an assumed ocean depth of 1000 m and conductivity of 4 S/m. The coefficients shown below should further be multiplied by a constant factor $a/2\pi$.

a_1^-	a_2^-	a_3^-	a_4^-	a_5^-	a_6^-	a_7^-	a_8^-	a_9^-	a_{10}^-	a_{11}^-	a_{12}^-
−2.360	−2.121	−0.365	0.436	0.053	−0.258	−0.019	0.175	0.009	−0.128	−0.005	0.099

a_1^*	a_2^*	a_3^*	a_4^*	a_5^*	a_6^*	a_7^*	a_8^*	a_9^*	a_{10}^*	a_{11}^*	a_{12}^*
−7.598	−3.544	−1.227	−0.203	0.125	0.107	−0.027	−0.068	0.006	0.048	0.001	−0.036

b_2^-	b_3^-	b_4^-	b_5^-	b_6^-	b_7^-	b_8^-	b_9^-	b_{10}^-	b_{11}^-	b_{12}^-
−4.724	0.485	−0.096	0.390	−0.588	−0.053	−0.056	−7.285	−2.316	0.065	0.144

b_2^*	b_3^*	b_4^*	b_5^*	b_6^*	b_7^*	b_8^*	b_9^*	b_{10}^*	b_{11}^*	b_{12}^*
−1.215	0.001	0.023	0.016	−18.381	0.004	−0.235	1.292	−1.492	−0.010	0.000

northern hemisphere and at about 35°-latitude in the southern hemisphere. There is accordingly a clear change of phase (reversal of sign) in the observed H variations beyond these focus latitudes in northern and southern hemispheres (see Fig. 2). These observations are in good agreement with those reported for the East Asian sector by Campbell and Schiffmacher (1985, 1988). An estimated current of 20 kA flows between adjacent contours and, also, the intensities of the focal currents in different seasons are different. Expectedly, the current intensities for the winter season (Fig. 5(a)) are the lowest of all the seasons. The current intensities at the northern and southern foci for the summer season (Fig. 5(c)) are about three times larger than those of the winter season. The difference between the values of the northern and southern foci indicates the *total* current intensity, which is about 300 kA, for the summer season. This is very high, when compared with the summer current intensities of other global regions (Malin and Gupta, 1977; Campbell and Schiffmacher, 1985). As observed in this study, Malin and Gupta (1977) also have reported a maximum intensity of current for Sq when its focus is located at mid-Pacific.

6.1.1 Westward lag of Sq focus Compared with the position of Sq foci in the North American and European regions, the Sq focus in the northern hemisphere in the East Asian sector is situated at a relatively lower latitude (Campbell and Schiffmacher, 1985). The mid-latitude pre-noon focus vortex of current, though not clearly seen in winter (Fig. 5(a)) and summer (Fig. 5(c)) seasons, is somewhat about 20–25 min. in the northern hemisphere, relative to the southern hemisphere in equinoctial season (Fig. 5(b)). By analyzing the IGY data of 1964–65, Malin and Gupta (1977) reported a westward lag for northern focus over the Pacific as 40 min, which is small, when compared to that seen over African region, about 105 min.

Two interesting features to note here are: (i) there is a maximum Sq focus current at mid-Pacific; and (ii) the minimum westward lag of Sq focus over the Pacific, which is about 20–25 min. Although the principal odd ($n - m = 1$) harmonic terms, P_2^1, P_3^2 and P_4^3, chiefly describe the overall nature of Sq, the combined even and odd n & m combination terms in calculating the current function (see equation 10 of Campbell and Schiffmacher, 1985) could be responsible for the pre-noon occurrence (westward tilt) of the northern Sq focus (Winch, 2002, personal communication). In such a case, a more detailed study of the even harmonic terms in the estimation of current function is further warranted. This would facilitate a better understanding of the greater lag of the Sq focus over a continental region (Africa) than over an oceanic region (Pacific), in addition to the changes in the ionospheric wind patterns over both these regions, as explained by Malin and Gupta (1977). Malin and Gupta (1977) attribute the westward tilt of the Sq focus to the differential frictional forces offered by land and ocean, with the former offering a larger frictional resistance than the latter to the ionospheric thermo tidal winds.

Table 3. Same as Table 2 except for the case when the self-induction effect of the ocean is *ignored*.

a_1^-	a_2^-	a_3^-	a_4^-	a_5^-	a_6^-	a_7^-	a_8^-	a_9^-	a_{10}^-	a_{11}^-	a_{12}^-
1.460	0.749	0.232	0.000	−0.029	0.000	0.009	0.000	−0.004	0.000	0.002	0.000

a_1^*	a_2^*	a_3^*	a_4^*	a_5^*	a_6^*	a_7^*	a_8^*	a_9^*	a_{10}^*	a_{11}^*	a_{12}^*
−9.102	−4.671	−1.445	0.000	0.179	0.000	−0.054	0.000	0.022	0.000	−0.011	0.000

b_2^-	b_3^-	b_4^-	b_5^-	b_6^-	b_7^-	b_8^-	b_9^-	b_{10}^-	b_{11}^-	b_{12}^-
−4.671	−2.285	0.000	0.468	0.000	−0.197	0.000	0.105	0.000	−0.064	0.000

b_2^*	b_3^*	b_4^*	b_5^*	b_6^*	b_7^*	b_8^*	b_9^*	b_{10}^*	b_{11}^*	b_{12}^*
−0.749	−0.366	0.000	0.075	0.000	−0.032	0.000	0.017	0.000	−0.010	0.000

6.2 Interpretation of the internal field variations, the oceanic effect and its implications on the mantle conductivity distribution

6.2.1 Separation of the observed field variations into external and internal parts It is seen from Fig. 4 that the external part of the field variations are well defined, when compared with the internal parts. This is the nature of the separated field variations at all the stations. This further shows that practically everywhere along the 210°MM region, the internal parts of the observed variations are severely contaminated, and hence are responsible for a large bias in the calculated EM induction response estimates (Table 1). The reasons for this could be many. First, as expected, some minor differences in the polynomial representation of the Fourier coefficients might have affected the internal field (Campbell and Schiffmacher, 1985). Second, the subsurface structure all along the western Pacific is highly heterogeneous and thus plays a dominant role in significantly affecting the induction. Third, as most of the observatories along the 210°MM region are either directly located over the Pacific Ocean or along the coastal regions of continents (e.g., Australian stations) (see Fig. 1), there is a possibility of strong influence of coupling of the internally induced oceanic currents with the underlying heterogeneous upper mantle, which is rather difficult to separate. Interestingly, the ocean has not shown any appreciable influence on the external parts of the field variations (Fig. 4). This explains that the Sq above the ocean is different from the Sq below the ocean.

6.2.2 Self-induction effect of the ocean on the induction by Sq Table 2 (Table 3) shows the coefficients for induction by the diurnal term of Sq when the self-induction effects of the ocean are not ignored (ignored). These coefficients are obtained after solving the simultaneous equations (equations 18 and 19) provided by Rikitake (1960), using the Gauss external *cosine* and *sine* P_2^1 coefficients given in Table A.1 of Appendix A. The coefficients listed in Tables 2 and 3 correspond to realistic values of depth of 1000 m and conductivity of 4 S/m for the ocean. In agreement with results reported by Rikitake (1960) (see tables 6 and 7 of his paper), our results also clearly show some notable differences between the coefficient values listed in Tables 2 and 3. This explains the fact that there persists a considerable influence of the self-induction effect of ocean on the EM induction response at 24-hr period. The coefficient values shown in Tables 2 and 3 should further be multiplied by the constant term, $a/2\pi$ where a, is the radius of the Earth.

Winch (1981) showed that at one cycle per day, the small Sq phase angle difference (*internal–external*) is about −2 degrees. This phase difference should be positive according to the theory of a solid uniform spherical conductor. However, under the influence of ocean, Winch (2002, personal communication) found that the phase angle difference changes to an alarming −16 degrees. Usually, because of the causal nature of the inducing (external) and induced (internal) fields, i.e., since the induced field lags behind the inducing one, the phase angle difference should be positive. This is true for the case of a purely one-dimensional (1-D) Earth in a nonoceanic region, where the conductivity varies only radially. However, for observatory data showing negative phase angles, two different types of interpretations are possible. Either the subsurface structure in the study region is not 1-D (and thus two or three-dimensional), or the ocean dynamo effect is dominant. It appears that, in the present case, both these interpretations are valid. As regards the former, it is well known that the subsurface structure all along the western Pacific is complex and highly heterogeneous, and is further coupled with the induced electric currents due to the passive oceanic self-induction effect. As regards the latter, it is interesting to observe here that the phase of the ocean dynamo is well ahead of the phase of the internal Sq field and thus their phase angle difference could be negative. Therefore, the presence of negative phase angles need not in general, be a consequence of induction (Winch, 1989) alone, in oceanic regions. It could well be associated with the strong oceanic dynamo effect.

As mentioned earlier (see Section 1), transients arise by self- and mutual induction within a circuit, when a system is suddenly disturbed, but they die out once a steady state is reached. However, since the external source current systems are continuously present across a wide range of spatial and temporal scales, the current system is never expected to reach a steady state! Therefore, the logic of a steady state system cannot be extended to the case of application of the Price's equation in modeling the induction response in hemispher-

ical thin sheets (Price, 1949), a theory on which Rikitake's (1960) theory, and in turn, the present analysis are based. Thus, we reiterate that ignoring the self-induction effect of the ocean while determining the induction response at periods of 1 day and below will lead to biased and improper estimation of the upper mantle electrical conductivity distribution in oceanic regions.

6.2.3 Interpretation of the derived induction response estimates In addition to the self-induction effect of the ocean, the other important factor that plays a vital role in vitiating the induction response is the presence of lateral inhomogeneities at upper mantle depths all along the western Pacific region. Table 1 shows the rough values of the average conductivity and depth estimates together with their errors and also phase estimates for the substitute conductor model determined for the period of Sq and its harmonics. Interestingly, although the depth estimates are consistent with the skin-depth relation, the conductivity estimates are not (and hence are described here as biased). Further, the responses at 12- and 8-hr periods show somewhat a more statistical consistency in the 'period-depth-conductivity' relationship (Table 1), compared with the responses of the other two periods. This appears to be a clear manifestation of the larger amplitudes seen at 12- and 8-hr periods compared to the amplitudes of 24- and 6-hr periods (Fig. 3). The phase angles are calculated as $\tan^{-1}(C_{imag}/C_{real})$ from the mean complex C-response given in column 2 of Table 1. The small phase angles, together with the derived response estimates at 12- and 8-hr periods also are compatible with the conditions prescribed by Weidelt (1972) for validity of the C-response. The mean depth to the substitute conductor is estimated to be 600 km in the 210°MM region, for 24-hr period. An average depth of 500 (700) km is usually expected for induction by Sq, when the effect of the induced currents in the ocean is removed (considered) (Takeda, 1991). Rikitake (1961) and Ashour (1971) showed that the oceanic influence on the induction is greatly reduced if a perfectly conducting core is situated at upper mantle depth. However, despite the reasonable agreement of the derived responses with their corresponding global estimates, they should still be considered only as rough estimates, particularly, since they are not modelled. The difficulty in modelling such response estimates is explained below. Thus, the rough response estimates and their errors given in Table 1 only provide rather a first-hand information as to how the self-induction effect of the ocean affects the Sq induction response in oceanic regions, particularly at periods of 1 day and below, where the effect of lateral inhomogeneities at upper mantle depths is dominant, as in the present case.

As for the region under investigation, the entire 210°MM region is tectonically very active, in the sense that the western Pacific stands as a locus of diverse tectonic activity that represents the largest intra-oceanic destructive plate margins in the world. This includes the ocean-ocean and ocean-continent collision zones. The Australian plate, by its continuous interaction with the Pacific plate, for example, has produced a complex array of oceanic to intra-continental extensional basins through sea-floor spreading. The subduction of the Philippine Sea plate south of the Japanese islands along the Ryuku arc trench forms a complex tectonic setting

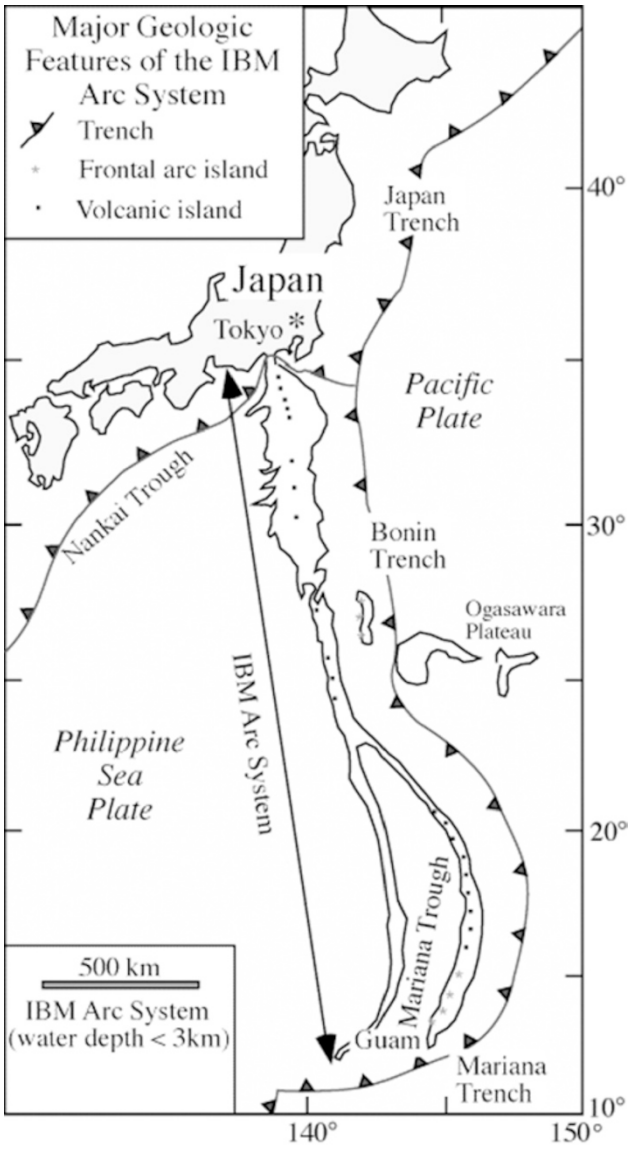

Fig. 6. Major tectonic settings and crustal section of the Izu-Bonin-Mariana (IBM) arc, along the 210°MM region. Figure shows the northern part of the arc system. Here also (as in Fig. 1), the map is drawn in geographic coordinates.

pattern that is active along the western Pacific region. Also, in the equatorial region in the 210°MM region, the Caroline ridge is surrounded by three major plates: the Pacific; the Philippine Sea; and the Australian plates. Further, there is also lithospheric convergence between the Pacific and the Philippine Sea plates along the Izu-Bonin-Mariana arc south of Japan (see Fig. 6). A more detailed map of the tectonic settings of the western Pacific is given by Parkinson and Pearce (1998).

Thus, a close proximity of such disparate tectonic settings has profound implications on topography, deformation and magmatism. A redistribution of aqueous and other fluids, transporting heat and solutes associated with these active plate margins also has a direct bearing on the electrical conductivity distribution at upper mantle depths in the western Pacific region. In view of this, it can be easily understood that the prime causes for severe contamination of the internal parts of the field variations (see Fig. 4) could be attributed

to the strong influences of lateral inhomogeneities and the EM coupling of the induced oceanic currents associated with them. The presence of such anomalous and complex subsurface structures poses a serious challenge to implement efficient numerical modelling algorithms and prevents us from determining a true conductivity-depth distribution model for the 210°MM region.

Also, the presence of the ocean, giving rise to large negative phase angles makes the 1-D modelling of the upper mantle electrical conductivity distribution difficult. As the complex pattern of the existing tectonic settings appear to be two- or three-dimensional in nature, the estimated C-responses cannot be used further for their subsequent modelling, as the formulation to calculate C-responses is essentially based on the assumption of a 1-D Earth (substitute conductor model). However, as mentioned earlier, in the present study, the C-responses were determined only to get rough estimates of conductivity and depth values in order to understand the bias in the EM induction response due to the presence of ocean. In fact, in such regions, where there is a strong lateral heterogeneity at upper mantle depths, the estimation of the geomagnetic *tensor* induction response, defined as the $\zeta(\omega)$-response, introduced by Zhang and Schultz (1992) might be more appropriate, since this new response function better resolves the upper mantle electrical conductivity. Incidentally, since the fully validated 3-D FEM forward solver of Weiss and Everett (1998) can readily calculate the $\zeta(\omega)$-response, such a response calculated for Sq periods over a realistic distribution of oceans and continents, as in the present case, can be aptly modelled following their approach and thus the electrical state of the upper mantle can be reasonably mapped.

7. Conclusions

The solution to Rikitake's (1960) hemispherical thin sheet model shows a considerable influence of the self-induction effect of the ocean on the EM induction response due to Sq. The present study, using more data sets from a unique network of observatories located along the 210°MM region confirms his theory on the role of the self-induction effect of the ocean on the derived Sq induction response for the study region. Although the analysis has brought out a well-defined external source current systems responsible for the generation of Sq field for all seasons, the coupling of electric currents induced in the ocean with the large-scale and complex tectonic structure of the upper mantle in the study region has been responsible for severe contamination of the internal part of the field variations, resulting in determination of biased induction response estimates. This confirms that Sq above the ocean is different to Sq below the ocean. The self-induction effects of the ocean cannot, as in the usual manner, be treated as 'transients' and neglected when the induction in hemispherical thin sheets is considered particularly at periods of 1 day and below. Also, since the presence of the ocean greatly influences Sq phase angles, it is difficult to get a reliable 1-D conductivity distribution in oceanic regions due to Sq. Thus, in such regions, perhaps an estimation of geomagnetic *tensor* induction response would be more appropriate to map the multi-dimensional complex tectonic structure of the upper mantle.

Acknowledgments. We thank the Ministry of Education, Science, Sports and Culture, Government of Japan for awarding the necessary research grants to carry out this work. One of the authors (EC) had the privilege of having a wide range of discussions on the role of oceans in Sq induction with Prof. Denis E. Winch. He earnestly thanks him for his kind help and stimulating discussions. He also thanks Prof. Y. Honkura for kindly discussing with him about the external source current systems of different seasons in the 210°MM region. EC is grateful to the directors of RCEP, DPRI for providing him with all the necessary facilities to carry out this work, while he was visiting Kyoto University, as a JSPS post-doctoral fellow and also to all his colleagues who have extended their kind cooperation throughout his stay there and made his life pleasant and comfortable. He thanks the JSPS foundation for awarding him a post-doctoral fellowship. The authors wish to thank Dr. Mark Everett and an anonymous referee for their meticulous reviews and helpful suggestions to improve the original version of the manuscript.

Appendix A.

Table A.1. External *cosine* and *sine* coefficients of first four principal harmonics of magnetic Sq potential in units of nT, for E (equinoctial)-season. n and m respectively denote the degree and order of the p_n^m harmonic terms.

p_n^m	*Cosine* coefficient	*Sine* coefficient
p_2^1	24.07	−3.89
p_3^2	−24.70	11.95
p_4^3	14.01	−10.88
p_5^4	−4.53	5.36

Appendix B.

Estimation of the coefficients listed in Tables 2 and 3 requires the solution of a set of simultaneous equations (see equations 18 and 19 of Rikitake (1960)), which in turn requires the generation of a set of R_{nN} and S_{nN} values, by solving the integrals,

$$R_{nN} = R_{Nn} = \int_0^1 P_n^1(x) \cdot P_N^1(x) dx$$

and

$$S_{nN} = S_{Nn} = \int_0^1 P_n^2(x) \cdot P_N^2(x) dx$$

as explained by Rikitake (1960) (see equations 15 and 17 in his paper). Here $P_n^m(x)$ denotes the Schmidt spherical surface harmonic of degree n and order m. The relation between $P_n^m(x)$ and the associated Legendre function, $P_{n,m}(x)$ is given by (Chapman and Bartels, 1940)

$$P_n^m(x) = P_{n,m}(x) \qquad \text{when} \quad m = 0 \quad \text{(B.1)}$$

$$p_x^m(x) = \left(\sqrt{\tfrac{2(n-m)!}{(n+m)!}}\right) P_{n,m}(x) \text{ when} \quad m > 0 \quad \text{(B.2)}$$

Using the relation expressed in (B.2), R_{nN} and S_{nN} can be calculated as

$$R_{nN} = \frac{\int_0^1 P_{n,1}(x) \cdot P_{N,1}(x)}{NF} \qquad \text{(B.3)}$$

and

$$S_{nN} = \frac{\int_0^1 P_{n,2}(x) \cdot P_{N,2}(x)}{NF} \qquad \text{(B.4)}$$

Table B.1. $R_{nN} = R_{Nn} = 12$ for $n \leq 12$ and $N \leq 12$.

$n\backslash N$	1	2	3	4	5	6	7	8	9	10	11	12
1	0.6667	0.433	0	−0.1318	0	0.0716	0	−0.0469	0	0.0338	0	−0.0258
2		0.4	0.1768	0	−0.0349	0	0.0143	0	−0.0076	0	0.0046	0
3			0.2857	0.1815	0	−0.0585	0	0.0335	0	−0.0228	0	0.0169
4				0.2222	0.1148	0	−0.0272	0	0.0124	0	−0.0071	0
5					0.1818	0.1155	0	−0.0378	0	0.0221	0	−0.0153
6						0.1538	0.0845	0	−0.0219	0	0.0106	0
7							0.1333	0.0848	0	−0.0279	0	0.0165
8								0.1176	0.0669	0	−0.0182	0
9									0.1053	0.067	0	−0.0221
10										0.0952	0.0553	0
11											0.087	0.0553
12												0.08

Table B.2. $S_{nN} = S_{Nn} = 12$ for $n \leq 12$ and $N \leq 12$.

$n\backslash N$	2	3	4	5	6	7	8	9	10	11	12
2	0.4	0.2796	0	−0.0924	0	0.05261	0	−0.0354	0	0.0261	0
3		0.2857	0.1353	0	−0.0292	0	0.0127	0	−0.0069	0	0.0043
4			0.2222	0.1432	0	−0.0472	0	0.0275	0	−0.019	0
5				0.1818	0.0967	0	−0.0239	0	0.0112	0	−0.0065
6					0.1538	0.0983	0	−0.0325	0	0.0191	0
7						0.1333	0.0745	0	−0.0197	0	0.0097
8							0.1176	0.075	0	−0.0248	0
9								0.1053	0.0604	0	−0.0167
10									0.0952	0.0607	0
11										0.087	0.0508
12											0.08

where, $NF = \left[\frac{1}{2}\sqrt{\frac{(n+m)!(N+m)!}{(n-m)!(N-m)!}}\right]$. In other words, the sets of R_{nN} and S_{nN} values will be obtained simply by first integrating the associated Legendre functions in the range of 0 to 1 and normalizing them with NF. It should be remembered that $m = 1$ in case of R_{nN} and $m = 2$ in case of S_{nN}. By solving (B.3) and (B.4), the values of R_{nN} and S_{nN} can be obtained as shown in Table B.1 and Table B.2 respectively.

References

Ashour, A. A., Electromagnetic induction in thin finite sheets having conductivity decreasing to zero at the edges with geomagnetic applications-II, *Geophys. J. Roy. Astr. Soc.*, **25**, 447–467, 1971.

Beamish, D., R. C. Hewson-Browne, P. C. Kendall, S. R. C. Malin, and D. A. Quinney, Induction in arbitrarily shaped oceans VI: Oceans of variable depth, *Geophys. J. Roy. Astr. Soc.*, **75**, 387–396, 1983.

Bullard, E. C. and R. L. Parker, Electromagnetic induction in the oceans, in *The Sea,* edited by E. C. Bullard and J. L. Worzel, Wiley, New York, Vol. 1, pp. 695–730, 1970.

Campbell, W. H. and R. S. Anderssen, Conductivity of the sub continental upper mantle: an analysis using quiet-day geomagnetic records of North America, *J. Geomag. Geoelectr.*, **35**, 367–382, 1983.

Campbell, W. H. and E. R. Schiffmacher, Quiet ionospheric currents of the northern hemisphere derived from geomagnetic field records, *J. Geophys. Res.*, **90**(A7), 6475–6486, 1985.

Campbell, W. H. and E. R. Schiffmacher, Quiet ionospheric currents of the southern hemisphere derived from geomagnetic records, *J. Geophys. Res.*, **93**, 933–944, 1988.

Chandrasekhar, E., Geo-electrical structure of the mantle beneath the Indian region derived from the 27-day variation and its harmonics, *Earth Planets Space,* **52**, 587–594, 2000.

Chandrasekhar, E. and S. Alex, On the anomalous features of the geomagnetic quiet-day field variations at Nagpur, India, *Geophys. J. Int.*, **127**, 703–707, 1996.

Chapman, S. and J. Bartles, *Geomagnetism,* Vol. II, 611 pp., Clarendon Press, Oxford, 1940.

Chapman, S. and T. T. Whitehead, The influence of electrically conducting material within the Earth on various phenomena of terrestrial magnetism, *Trans. Camb. Phil. Soc.*, **22**, 463–482, 1923.

Fainberg, E. B., Electromagnetic induction in the world ocean, *Geophys. Surv.*, **4**, 157–171, 1980.

Fainberg, E. B., A. V. Kuvshinov, and B. Sh. Singer, Electromagnetic induction in a spherical Earth with non-uniform oceans and continents in electric contact with the underlying medium—I: Theory, method and examples, *Geophys. J. Int.*, **102**, 273–281, 1990a.

Fainberg, E. B., A. V. Kuvshinov, and B. Sh. Singer, Electromagnetic induction in a spherical Earth with non-uniform oceans and continents in electric contact with the underlying medium—II: Bimodal global geomagnetic sounding of the lithosphere, *Geophys. J. Int.*, **102**, 283–286, 1990b.

Kendall, P. C. and D. A. Quinney, Induction in the oceans, *Geophys. J. Roy. Astr. Soc.*, **74**, 239–255, 1983.

Kuvshinov, A. V., D. B. Avdeev, and O. V. Pankratov, Global induction by Sq and Dst sources in the presence of oceans: bimodal solutions for non-uniform spherical surface shells above radially symmetric earth models in comparison to observations, *Geophys. J. Int.*, **137**, 630–650, 1999.

Larsen, J. C., Electric and magnetic fields induced by deep sea tides, *Geophys. J. Roy. Astr. Soc.*, **16**, 47–70, 1968.

Malin, S. R. C., The effect of the sea on lunar variations of the vertical component of the geomagnetic field, *Planet. Space Sci.*, **17**, 487, 1969.

Malin, S. R. C., Separation of the lunar daily geomagnetic variations into parts of ionospheric and oceanic origin, *Geophys. J. Roy. Astr. Soc.*, **21**, 447–455, 1970.

Malin, S. R. C. and J. C. Gupta, The Sq current system during the International Geophysical Year, *Geophys. J. Roy. Astr. Soc.*, **49**, 515–529, 1977.

Maus, S., R. H. Tyler, and H. Luehr, Ocean tidal dynamo identified in CHAMP satellite magnetic data, AGU Fall Meeting Abstracts, GP61A-1017, F407, 2002.

Olsen, N., The electrical conductivity of the mantle beneath Europe derived from C-responses from 3 to 720 hrs, *Geophys. J. Int.*, **133**, 298–308, 1998.

Parkinson, I. J. and J. A. Pearce, Peridotites from the Izu-Bonin-Mariana Forearc (ODP Leg 125): Evidence for a mantle melting and melt-mantle interaction in a supra-subduction zone setting, *Journal of Petrology,* **39**, 1577–1618, 1998.

Price, A. T., The induction of electric currents in non-uniform thin sheets and shells, *Quart. Jour. Mech., Appl. Math,* **2**, 283–310, 1949.

Rangarajan, G. K., Indices of geomagnetic activity, in *Geomagnetism,* edited by J. A. Jacobs, Vol. 3, pp. 323–384, Academy Press, 1989.

Rikitake, T., Electromagnetic induction in a hemi-spherical ocean by Sq, *J. Geomag. Geoelectr.*, **11**, 65–79, 1960.

Rikitake, T., The effects of ocean on rapid geomagnetic changes, *Geophys. J. R. Roy. Astr. Soc.*, **5**, 1–15, 1961.

Schmucker, U., Anomalies of geomagnetic variations in south-western United States, *Bull. Scripps Inst. Oceanogr.*, **13**, 1–165, 1970.

Schmucker, U., Substitute conductors for electromagnetic response estimates, PAGEOPH, **125**, 341–367, 1987.

Schmucker, U., Spherical harmonic analysis of solar daily variations in the years 1964–1965: Response estimates and source fields for global induction—I. Methods, *Geophys. J. Int.*, **136**, 439–454, 1999.

Spiegel, M. R., Schaum's Outline of Theory and Problems of Fourier Analysis, *Schaums's outline series,* pp. 22, McGraw-Hill Book Company, USA, 1974.

Takeda, M., Electric currents in the ocean induced by the geomagnetic Sq field and their effects on the estimation of mantle conductivity, *Geophys. J. Int.*, **104**, 381–387, 1991.

Weidelt, P., The inverse problem of geomagnetic induction, *J. Geophys.*, **38**, 257–289, 1972.

Weiss, C. J. and M. E. Everett, Geomagnetic induction in a heterogeneous sphere: fully threedimensional test computations and the response of a realistic distribution of oceans and continents, *Geophys. J. Int.*, **135**, 650–662, 1998.

Wessel, P. and W. H. F. Smith, New version of the generic mapping tools released, *EOS Trans. AGU,* **76**, 329, 1995.

Winch, D. E., Spherical harmonic analysis of geomagnetic tides, 1964–1965, *Phil. Trans. R. Soc. Lond.*, **303A**, 1–104, 1981.

Winch, D. E., Induction in a model ocean, *Phys. Earth Planet Inter.*, **53**, 328–336, 1989.

Yumoto, K. and the 210°MM Magnetic Observation Group, The STEP 210° Magnetic meridian network project, *J. Geomag. Geoelectr.*, **48**, 1297–1309, 1996.

Zhang, T. S. and A. Schultz, A 3-D perturbation solution for the EM induction problem in a spherical Earth—the forward problem, *Geophys. J. Int.*, **111**, 319–334, 1992.

E. Chandrasekhar (e-mail: esekhar24@yahoo.co.in), N. Oshiman, and K. Yumoto